Mon. Not. R. Astron. Soc. **000**, 000–000 (0000) Printed 5 February 2008 (MN LaTeX style file v2.2)

arXiv:astro-ph/0602466v1 21 Feb 2006

Tracing gas motions in the Centaurus cluster

J. Graham[1]*, A.C. Fabian[1], J.S. Sanders[1] and R.G. Morris[1,2]
[1] *Institute of Astronomy, Madingley Road, Cambridge*
[2] *Kavli Institute for Particle Astrophysics and Cosmology, Stanford Linear Accelerator Center, Stanford, CA 94305-4060, USA*

5 February 2008

ABSTRACT

We apply the stochastic model of iron transport developed by Rebusco et al. (2005) to the Centaurus cluster. Using this model, we find that an effective diffusion coefficient D in the range $2 \times 10^{28} - 4 \times 10^{28}\,\mathrm{cm^2 s^{-1}}$ can approximately reproduce the observed abundance distribution. Reproducing the flat central profile and sharp drop around $30 - 70$ kpc, however, requires a diffusion coefficient that drops rapidly with radius so that $D > 4 \times 10^{28}\,\mathrm{cm^2 s^{-1}}$ only inside about 25 kpc. Assuming that all transport is due to fully-developed turbulence, which is also responsible for offsetting cooling in the cluster core, we calculate the length and velocity scales of energy injection. These length scales are found to be up to a factor of ~ 10 larger than expected if the turbulence is due to the inflation and rising of a bubble. We also calculate the turbulent thermal conductivity and find it is unlikely to be significant in preventing cooling.

Key words: cooling flows – galaxies: clusters: general – galaxies: clusters: individual: Centaurus

1 INTRODUCTION

Galaxy clusters contain bright, extended, sources of X-ray emission. This emission is primarily thermal bremsstrahlung in the low-density ($\sim 10^{-3}\,\mathrm{cm^{-3}}$), optically-thin plasma of the IntraCluster Medium (ICM), gravitationally heated to $10^7 - 10^8$ K in the cluster dark matter potential. Spectroscopic observations have revealed the ICM to be enriched with metals ejected from the cluster galaxies with an average background metallicity of about a third solar (Edge & Stewart 1991). Observations show that this value is constant out to a redshift of $z \sim 1$ (Mushotzky & Loewenstein 1997; Hashimoto et al. 2004) and a comparison of the abundance distribution with supernova models has led to the conclusion that this background enrichment is the result of type II supernova activity early in the cluster's history (e.g. Finoguenov et al. 2000; Tozzi et al. 2003).

Two distinct classes of cluster have been identified based on their X-ray surface brightness profile. Cool-core clusters are characterised by a bright peak in their X-ray surface brightness profile, which is not present in non-cool-core clusters. The cool-core clusters are believed to correspond to dynamically relaxed systems, i.e. those which have not undergone a recent merger. The ICM cooling timescale in these bright central regions is often much shorter than the Hubble time. It was expected that this short cooling time would result in the deposition of large amounts of cool gas that would be observed in these regions — the cooling flow model (e.g. Fabian 1994). However, detailed observations of clusters have failed to locate gas below about a third of the mean cluster temperature (e.g. Allen et al. 2001; Peterson et al. 2003; Sanders et al. 2004; Voigt & Fabian 2004) and it is now widely believed that some form of distributed heating must be taking place.

A wide range of solutions to the cooling flow problem have been proposed (see Peterson & Fabian 2005, for a review), with most of the attention focused on energy injection by the central Active Galactic Nucleus (AGN). These models have the advantage that the AGN is able to provide enough power to offset the cooling (Tabor & Binney 1993; Churazov et al. 2002); however, it is unclear how the energy can be distributed to provide enough heating over the entire cooling region. A clue may be provided by the observation of bubbles of synchrotron-emitting plasma in many cool-core clusters (e.g. Böhringer et al. 1993; Sanders & Fabian 2002; McNamara et al. 2000; Bîrzan et al. 2004). These are inflated by jets emanating from the central AGN. Some clusters show evidence for further "ghost" bubbles at larger radii (e.g. Fabian et al. 2002). These show weak, low-frequency, radio emission and are presumably the result of an earlier epoch of AGN activity. This has led to much work on the possibility that the inflation and subsequent rise of these bubbles through the cluster atmosphere is responsible for the transfer of energy from AGN to ICM (e.g. Fabian et al. 2003a; Mathews et al. 2003; Ruszkowski et al. 2004).

There is speculation that cluster heating might be driven by turbulent motion of the cluster gas. Evidence for a Kolmogorov-type turbulent cascade has been found in the pressure fluctuation spectrum of Coma (Schuecker et al. 2004) and in the Faraday rotation power spectrum of Hydra A (Vogt & Enßlin 2005). However, the level of turbulence in cool-core clusters remains unclear; the observation of extended, linear Hα filaments in several cool-core

---

* E-mail:jgraham@ast.cam.ac.uk

© 0000 RAS

clusters has been used as evidence that the ICM in these systems cannot be fully turbulent (Fabian et al. 2003b).

A method of quantifying the level of stochastic motions in cool-core clusters was developed and applied to the Perseus cluster by Rebusco et al. (2005). Their method is based on the central metallicity peak observed in cool-core clusters which is absent in non-cool-core systems (Fukazawa et al. 2004; De Grandi et al. 2004). This is likely a result of metal ejection by the Brightest Cluster Galaxy (BCG). The abundance profile does peak on the BCG, but does not match the light profile in detail. By assuming the difference in these profiles to be the result of diffusion of metals caused by stochastic motions in the cluster gas, Rebusco et al. (2005) were able to determine the diffusion coefficient; $D = 2\times10^{29}\,\mathrm{cm^2 s^{-1}}$ for the Perseus cluster. Linking this with a model of turbulent heating, and assuming heating balanced cooling, they predicted the length and velocity scales of the gas motion as $l \sim 10\,\mathrm{kpc}$ and $v \sim 300\,\mathrm{km\,s^{-1}}$.

Here we apply the model of Rebusco et al. (2005) to the case of the Centaurus cluster. Centaurus is unusual in showing super-solar abundances near the centre - the peak metallicity is around 2 compared with about 0.7 for Perseus - making it an interesting limiting case for the model.

We adopt the cosmology $H_0 = 70\,\mathrm{km\,s^{-1}\,Mpc^{-1}}$, $\Omega_m = 0.3$, $\Omega_\Lambda = 0.7$ and use the solar abundances of Anders & Grevesse (1989) throughout.

2 DIFFUSION MODEL

We employed the model for iron transport developed in Rebusco et al. (2005). This is based on a combined diffusion-advection equation in which the advection term ensures that the equations satisfy the physical constraint that a spatially uniform abundance undergoes no evolution in the absence of sources:

$$\frac{\partial n_H a}{\partial t} = \nabla\cdot(n_H D \nabla(a)) + S, \qquad (1)$$

n_H is the ICM hydrogen density, a is the abundance, D is the diffusion coefficient and S the (spatially distributed) sources of iron.

The model of iron injection is taken from Böhringer et al. (2004) and considers two sources of iron; type Ia supernovae and stellar winds. In each case, it is assumed that the rate of injection was greater in the past when the stellar population of the BCG was younger and that the change in time can be approximated using the power law model of Renzini et al. (1993) leading to source terms of the form:

$$S_{\mathrm{SN}} = 0.7\times10^{-12}\times SR \times \left(\frac{t}{t_h}\right)^{-k} \left(\frac{L_B(r)}{L_{B\odot}}\right) \mathrm{M_\odot yr^{-1}}, \qquad (2)$$

$$S_{\mathrm{Stellar}} = 7\times10^{-14} \left(\frac{t}{t_h}\right)^{-1.3} \left(\frac{L_B(r)}{L_{B\odot}}\right) \mathrm{M_\odot yr^{-1}}. \qquad (3)$$

Here $L_{B\odot}$ and $\mathrm{M_\odot}$ refer to the solar B-band luminosity and mass, respectively, t_h is the Hubble time, SR is the supernova rate in SNU (one SNU is the rate of supernovae explosions such that a galaxy with $10^{10}L_{B\odot}$ has one SN per century), k controls the rate of type IA supernovae in the past and L_B describes the luminosity profile of the galaxy. The model parameters k, SR and the total integration time are not known. We expect k in the range $1.1-2$ (Böhringer et al. 2004). The integration time is interpreted as the time since the last major cluster merger, as such a process would have a disruptive effect on the abundance peak. This time together with the values of k and SR are subject to the constraint that the total mass injected match the observed excess in the cluster. Following Rebusco et al. (2005), we take $k = 1.4$, integrate for 8 Gyr and fix the supernova rate at 0.19 SNU to match the observed mass excess.

In addition to iron injection, there will be evolution of the ICM hydrogen density with time; for example, stellar mass-loss liberates hydrogen as well as heavy elements, and merging subsystems will have gas stripped. We neglect these effects and regard the hydrogen density as a constant in all our models.

3 MODELLING DIFFUSION IN CENTAURUS

3.1 Properties of the Centaurus Cluster

High resolution X-ray imaging of the core of the Centaurus cluster has revealed a complex, asymmetric, structure with a wealth of small-scale features (Fabian et al. 2005). For our purposes it is sufficient to consider a spherically symmetric profile. In order to construct an accurate profile over a wide range of cluster radii, we have combined data from several observations of Centaurus. The highest resolution *Chandra* data is only available for the inner $\sim 60\,\mathrm{kpc}$ of the cluster and so we have supplemented this with a new reduction of archival *XMM-Newton* data out to $\sim 100\,\mathrm{kpc}$ and published deprojections of data from the *ROSAT* (Allen & Fabian 1994) and *ASCA* (White 2000) satellites at larger radii.

3.1.1 Data Reduction

We analysed *Chandra* observation IDs 0504, 0505, 4954, 4955 and 5310. Each observation placed the centre of the cluster near the aim-point of the ACIS-S3 CCD. The dataset was reprocessed using CIAO and the latest appropriate gain file (acisD2000-01-29gain_ctiN0003.fits). Flares in the datasets were filtered by using the $2.5-7\,\mathrm{keV}$ count rate on the ACIS-S1 CCD (which is back-illuminated like the S3 CCD), and the LC_CLEAN tool. This yielded a total exposure time of 196 ks. The event files were reprojected to match the longest observation (4954). Standard blank-sky observations were tailored to match the individual observations, and then reprojected to match 4954. The exposure time in each background observation was adjusted so that the count rate in the $9-12\,\mathrm{keV}$ band matched the cluster observation, to account for the gradual increase in background with time.

In each annulus, spectra and background spectra were extracted from each of the datasets and blank-sky observations. Weighted response matrices were generated for each of the different observations using MKACISRMF, and weighted ancillary responses created using MKWARF. The extracted spectra in the annulus were added together. We took the background spectra for each of the datasets. The exposure time of the spectra were effectively reduced by discarding photons. The exposure times were reduced so that the fractional time of each background observation to the total exposure time of the background spectrum matched the fractional time of each observation to the total exposure time of the total foreground spectrum. This procedure also optimised for the longest total background exposure time. The shortened background spectra were added together to create a total background. The responses were added together, with weighting according to the number of counts as before.

The spectra were fit using the PROJCT model in XSPEC Arnaud (1996) to account for projection. A VMEKAL (Mewe et al. 1985; Liedahl et al. 1995) model was used to compute the emission spectra. In the fit the Galactic absorption was a free parameter. In each shell, the temperature, normalisation, O, Ne, Si, S, Ar, Ca, Fe and Ni abundances were free parameters. The model was fit between 0.5 and 7 keV, minimising the χ^2 statistic.

To obtain the 1D profile from the *Chandra* observations, we averaged over a 93.9-degree sector to the west of the centre, so avoiding the swirl of cool gas seen to the east (Fabian et al. 2005).

The *XMM-Newton* data were reduced in standard fashion. High-energy ($10-15$ keV), single pixel (`PATTERN == 0`) light curves were constructed in 100-second bins for the events satisfying the FLAGs `#XMMEA_EM` / `#XMMEA_EP` for the MOS / pn, respectively. Count-rate cuts of $0.15/0.45$ ct s^{-1} were applied for the two instruments. This results in 31 ks of good time for the MOS, but zero for the pn due to background flaring.

The region between $0-150$ kpc was divided into 10 annuli with equal net counts. Background spectra were extracted from the blank-sky fields of Read & Ponman (2003), and normalised using the ratio of the count-rate outside the field of view for the science to background observations. The results presented are from MOS1 only. The model was `projct*phabs(mekal)` with a common, free abundance, and spectra were fitted over the range $0.5-7.5$ keV.

3.1.2 *Adopted profiles*

The deprojected iron abundance profile used is shown in Fig. 1. We have removed data-points corresponding to a central abundance decrease. Such an "abundance hole" could be due to the gas being multiphase. If it is real, it will certainly require some additional physical process beyond diffusion from a centrally concentrated source, e.g. the radial gas motion associated with bubble formation (Churazov et al. 2004). We have fitted a model profile of the form:

$$a = 0.3\frac{19.2+\left(\frac{r/\mathrm{kpc}}{33.4}\right)^{4.55}}{2.95+\left(\frac{r/\mathrm{kpc}}{33.4}\right)^{4.55}}a_\odot. \qquad (4)$$

The deprojected hydrogen density profile is shown in Fig. 2 with the adopted fit of the form:

$$n_H = \left(\frac{r/\mathrm{kpc}}{0.096}\right)^{-0.87} - 0.00055\,\mathrm{cm}^{-3}. \qquad (5)$$

It has been assumed that the electron and hydrogen densities are related as $n_e = 1.2n_H$. The deprojected temperature profile is shown in Fig. 3, with a powerlaw fit of the form:

$$T = 0.72\left(\frac{r}{\mathrm{kpc}}\right)^{0.38}\mathrm{keV}, \qquad (6)$$

which is valid over the range $1 < r < 100$ kpc.

3.2 Properties of NGC 4696

NGC 4696 is the brightest cluster galaxy of the Centaurus cluster and is situated at the centre of the abundance peak. We derive the luminosity of NGC 4696 from the integrated photometry presented in the HYPERLEDA catalogue (Paturel et al. 2003). The total B-band magnitude is given as B $= 11.51 \pm 0.01$, uncorrected for absorption, and B $= 11.03$ with the stated correction for galactic B-band extinction. Hence we adopt a *B*-band luminosity for NGC 4696 of $1.2\times10^{11}L_\odot$. The luminosity profile was taken to be a Hernquist (1990) profile with a scale radius of 9.9 kpc chosen to match the radius containing 50 per cent of the total *B* light in Lauberts & Valentijn (1989).

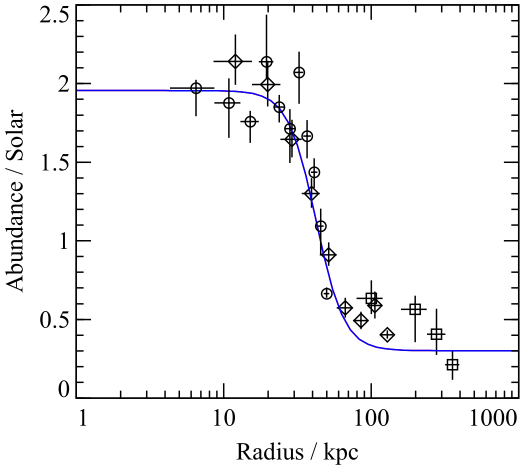

Figure 1. Deprojected iron abundance profile for the Centaurus cluster. The data is from *Chandra* (circles), *XMM-Newton* (diamonds) and *ROSAT* (squares). *Chandra* data for the inner 5 kpc (where an abundance hole is observed) has been excluded. The solid line represents a fitted profile with a background abundance of 0.3 solar, adopted through the remainder of the work.

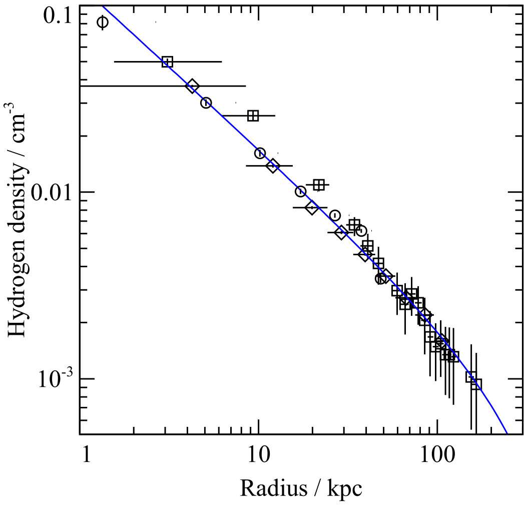

Figure 2. Deprojected hydrogen density with data from *Chandra* (circles), *XMM-Newton* (diamonds) and *ROSAT* (squares). The solid line is a powerlaw fit

.

4 RESULTS

Fig. 5 shows the abundance profile produced by simulations using spatially uniform diffusion coefficients of $2\times10^{28}\,\mathrm{cm}^2\mathrm{s}^{-1}$, $4\times10^{28}\,\mathrm{cm}^2\mathrm{s}^{-1}$ and $2\times10^{29}\,\mathrm{cm}^2\mathrm{s}^{-1}$. For comparison, Fig. 4 shows the abundance profile in the absence of diffusion. $D =$

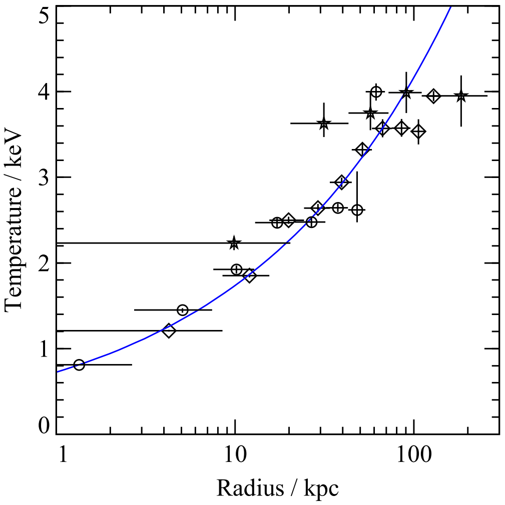

Figure 3. Deprojected temperature profile for the Centaurus cluster with data from *Chandra* (circles), *XMM-Newton* (diamonds) and *ASCA* (stars) The solid line is a simple power-law fit to the profile. This form provides a good fit in the inner 100 kpc of the cluster but may not be accurate outside this region.

$4\times10^{28}\,\mathrm{cm}^2\mathrm{s}^{-1}$ provides a reasonable fit to the observed abundance profile in the central regions, although the model significantly underestimates the iron abundance at higher radii, whilst $D = 2\times10^{28}\,\mathrm{cm}^2\mathrm{s}^{-1}$ provides a better fit at outer radii but is a poor fit within 20 kpc of the core. These values of D are factors 5 and 10 times lower than the value of $D = 2\times10^{29}\,\mathrm{cm}^2\mathrm{s}^{-1}$ found for Perseus by Rebusco et al. (2005) and are consistent with the limit $D < 6\times10^{28}\,\mathrm{cm}^2\mathrm{s}^{-1}$ derived by Fabian et al. (2005) based on the width of the abundance peak and the local sound crossing time.

4.1 Variable diffusion coefficient

Rebusco et al. (2005) find that the abundance profile becomes more “boxy” when the diffusion coefficient declines as a function of radius. This can be understood, as the large diffusion coefficient near the cluster centre causes metals to be rapidly spread to larger radii where they accumulate. For the Perseus cluster, there is no clear evidence that such a model reproduces the observed abundance distribution. In Centaurus, however, the high central abundance region is more sharply cut off, indicating that such a model might be favoured. Here, we consider fiducial models of the form proposed by Rebusco et al. (2005):

$$D = D_0\left(\frac{n_H(r)}{n_H(r_0)}\right)^{\alpha}, \qquad (7)$$

with r_0 being a characteristic scale radius at which the diffusion coefficient is D_0, and α controlling how centrally concentrated the diffusion coefficient is (larger values of α correspond to more centrally concentrated diffusion coefficients). However, such models may lead to unphysical values of the diffusion coefficient in some areas of the cluster and so we impose the additional constraint that $D \leqslant 0.11 c_s r$ where c_s is the local sound speed. The numerical factor is taken from the turbulent diffusion simulations of Dennis & Chandran (2005) that are discussed in Section 5.1.

Fig. 6 shows abundance profiles with values of α from -1 to 3 and a scale radius of 25 kpc. It can be seen that the flat inner profile and sharp curvature around $30-40$ kpc is better matched with increasing values of α. This is consistent with a picture where the energy driving the turbulent motion is injected at the cluster centre, possibly by the inflation and subsequent buoyant rise of the radio bubbles.

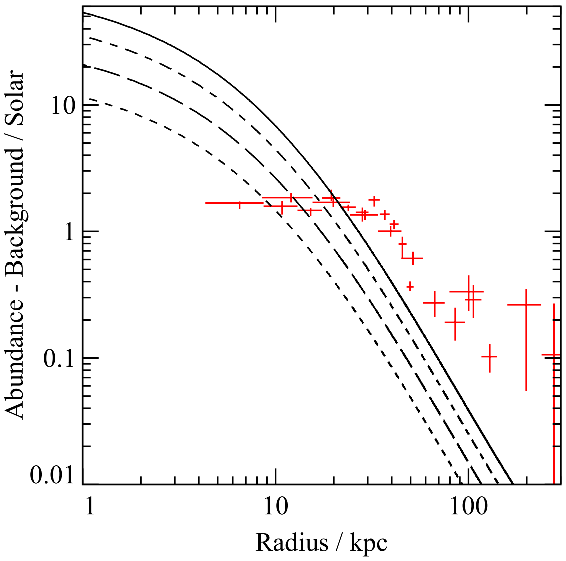

Figure 4. Background-subtracted abundance profile in the absence of any diffusion; i.e. when the abundance follows the BCG light. Points represent the data, as in figure 1, whilst lines represent the model at times of 1,2,4 and 8 Gyr.

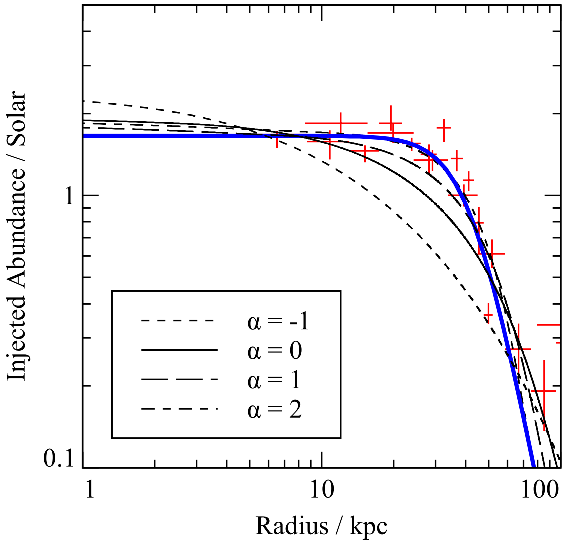

Figure 6. Variable diffusion coefficient model at an age of 8 Gyr with $D = 4\times10^{28}\,\mathrm{cm}^2\mathrm{s}^{-1}\,{\frac{n(r)}{n(r_0)}}^{\alpha}$, $r_0 = 25$ kpc, $\alpha = -1$ (dots), $\alpha = 0$ (solid) $\alpha = 1$ (dashed) $\alpha = 2$ (dot-dashed) and background-subtracted model (thick solid line). Models with increasing values of α provide an improved fit to the data points.

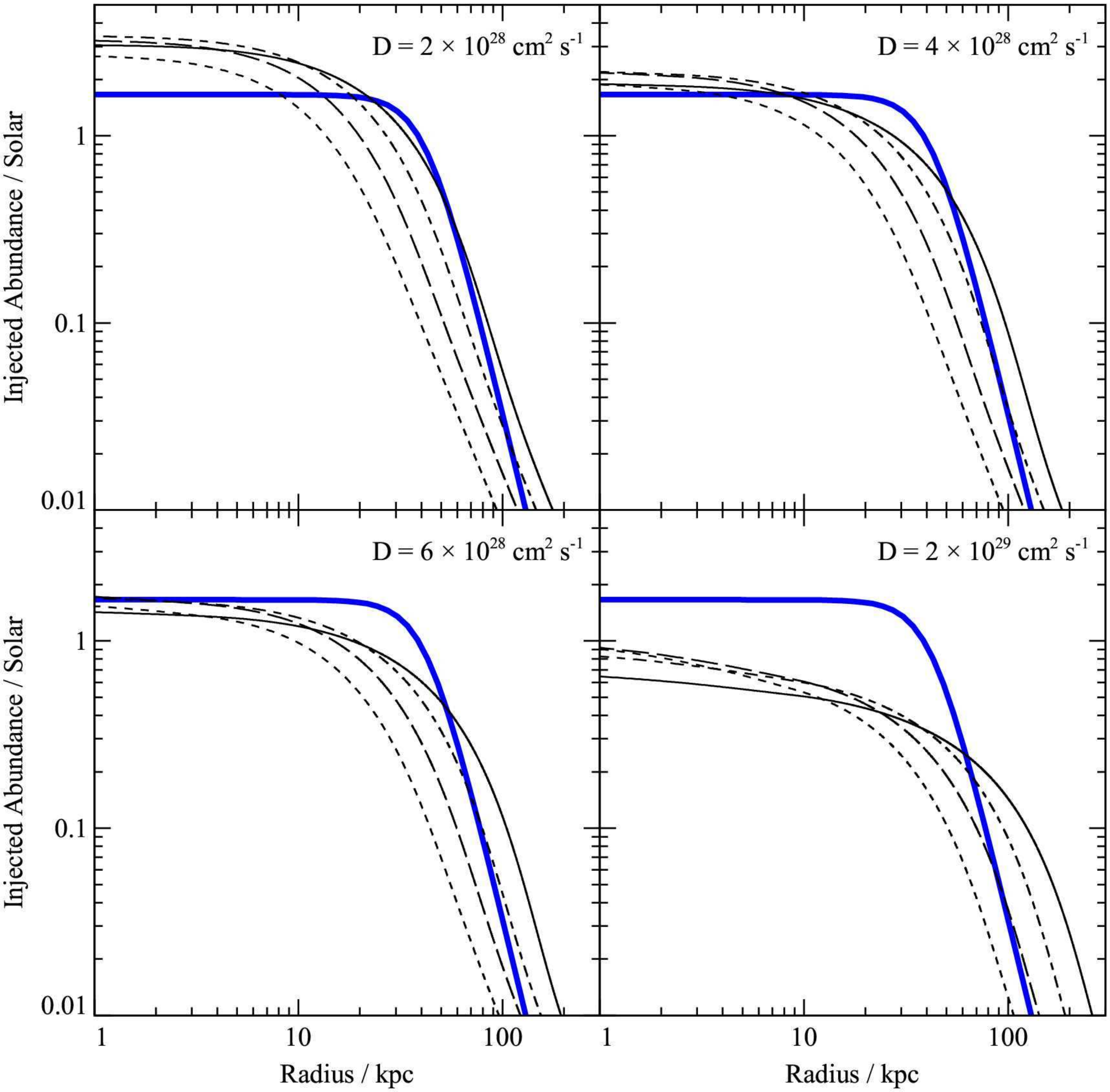

Figure 5. Simulations with constant diffusion coefficients of $2 \times 10^{27}\,\mathrm{cm^2 s^{-1}}$, $2 \times 10^{28}\,\mathrm{cm^2 s^{-1}}$, $4 \times 10^{28}\,\mathrm{cm^2 s^{-1}}$ and $2 \times 10^{29}\,\mathrm{cm^2 s^{-1}}$ at times of 1, 2, 4 and 8 Gyr (dotted, dashed, dot-dashed and solid lines respectively) and background-subtracted model (thick solid line).

5 TURBULENT HEATING OF CLUSTER GAS

The dissipation of energy contained in turbulent motions of the cluster gas may act as a significant heat source in the ICM. This process can provide the kind of spatially extended source of heat that is needed to balance cooling over the entire cooling radius of the cluster. There are two distinct sources for such energy; the merging of sub-clusters and energy injection through the central AGN. These processes differ in the expected length scales of the energy injection. In the case of mergers, this scale can be comparable to the size of the cluster, whilst in the case of AGN activity, the scale will be much smaller, limited to the size of the radio bubbles. Turbulence may also produce heating by mixing of hotter gas into the cooler regions, i.e. turbulent conduction (e.g. Cho et al. 2003; Voigt & Fabian 2004).

5.1 Heating by dissipation

On dimensional grounds, a diffusion coefficient may be written as $D = C_1 vl$ where v and l are velocity and length scales relevant to the diffusion process and C_1 is a constant, typically of order unity. By a similar argument, the simplest possible expression for the rate of heating due to dissipation turbulent motions is $\Gamma = C_2 \rho v^3/l$, where

ρ is the gas density and v and l are the energy injection scales of the turbulence, assumed to be the same as the scales of the diffusive motions. If we adopt these expressions and assume the cluster cooling to be entirely balanced by turbulent dissipation, we may write:

$$\Lambda[T(r),a(r)]n(r)^2 = \frac{C_2\rho(r)v(r)^3}{l(r)}, \tag{8}$$

where $\Lambda(T,Z)$ is the cooling function. To fix the constants C_1 and C_2 we take the values given in Dennis & Chandran (2005); $C_1 = 0.11$ and $C_2 = 0.4$. In practise, Equation 8 is an upper limit on the required turbulent heating, as any process that induces turbulent motion will also provide other heating. Observations show both weak shocks and sound waves associated with rising bubbles which will provide additional distributed heating.

Fig. 7 shows the calculated length and velocity scales of the turbulent motions required to balance cooling, given the variation in D with radius. The cooling function was calculated using the MEKAL plasma emission code (Mewe et al. 1985; Liedahl et al. 1995), assuming that the ratio of all heavy element abundances to solar follow that of iron. At the scale radius, the models have a scale length of about 4 kpc and a velocity of about 150 $\mathrm{kms^{-1}}$. The models with α larger than 0 show an initial rise in the length scale of turbulent motions — this is over the region where the diffusion coefficient is limited by the requirement that $D \leqslant 0.11 r c_s$ — and is the region in which the diffusion approximation is least reliable. Outside this inner region, the rapid drop-off in both length and velocity scales is again consistent with a picture of turbulent energy being injected into the cluster core and dissipating away from this region.

Using the calculated length and velocity scales, we may make a comparison of the implied turbulent viscosity with the standard Spitzer (1956) viscosity for a hydrogen plasma, assuming that the appropriate turbulent viscosity is of the form $\mu = \alpha\rho v l$. Using $vl = D/0.11$ and the cluster properties at a radius of 25 kpc, the Spitzer viscosity is $2.5\times10^2\,\mathrm{g\,cm^{-1}\,s^{-1}}$, and the turbulent viscosity $\mu = 4.5\times10^3\alpha$, so the turbulent viscosity exceeds the ion viscosity for any $\alpha > 0.06$.

It is notable that, in all the models, the length scale of the turbulence rises a factor of more than 3 above the mean radius measurement for the Centaurus bubbles of 1.37 kpc from Dunn & Fabian (2004). If we consider this bubble radius as the upper bound on the energy injection radius $l_{\max} = 1.37$ kpc, then $v(r) \geqslant D(r)/0.11 l_{\max}$. Fig. 8 shows the heating as a fraction of the cooling rate and the velocity as a fraction of the local sound speed assuming $l = l_{\max}$ everywhere. The effect on the calculated heating rate and velocity distribution is shown in Fig. 8. Since the heating rate at fixed D varies as l^{-4}, fixing the injection scale of the turbulence to be small causes large increases in the calculated heat injected. For models with $\alpha > 0$, it also requires that the gas velocity be strongly supersonic in order to maintain the diffusion coefficient in the cluster centre. In practise, the supersonic velocities are in a regime where the simple model of turbulence we have used does not apply and shock waves would presumably damp such motions quickly. Nevertheless, such supersonic motions and large heat excesses are not observed in the cluster core, which suggests that bubble-injected turbulent motions may not be able to reproduce the observed abundance distribution.

For comparison, Fig. 9 shows the same information for the Perseus cluster, based on the results of Rebusco et al. (2005), who did not find any reason to favour the $\alpha > 0$ results over the simple $\alpha = 0$ uniform diffusion coefficient. The value of $l_{\max}$ is fixed at 8.52 kpc based on the average inner bubble radius from Dunn & Fabian (2004). In the case of Perseus, the model does not produce supersonic velocities, at least for the case of a uniform diffusion coefficient. Application of the technique to a larger sample of clusters would be needed to show whether the problems seen in Centaurus are a special feature of that cluster.

It is clear that reproducing the observed abundance distribution with a diffusion model requires both a large diffusion coefficient at the centre and a relatively small coefficient ($D \lesssim 4\times10^{28}\,\mathrm{cm^2 s^{-1}}$) at radii of about 25 kpc to prevent spreading of the sharp abundance edge. On the assumption that turbulence is produced by the rising bubbles, this situation is hard to reconcile with the presently observed bubble properties. This may be because the presently observed bubbles are not representative of those produced during the lifetime of the cluster; if previous generations of bubbles have been substantially larger, the diffusion coefficient can be maintained with lower gas velocities. However the power required to inflate the bubbles scales as r^2_{bubble} and so the increase in bubble radius required to bring the diffusive velocity under the sound speed under the assumptions used in Fig. 8 would require more than an order of magnitude increase in jet luminosity in the models with $\alpha > 0$.

The difficulties may also be avoided if the turbulence is produced by a different mechanism, e.g. focusing of sound waves produced in sub-cluster mergers (Pringle 1989). Centaurus is believed to be undergoing a merger (Churazov et al. 1999). If this merger is affecting the abundance distribution, for example by causing the sharp truncation of a naturally extended profile, comparison of the diffusive models to the observed distribution will be misleading.

If the merger has not affected the abundance distribution, we must consider the possibility that some process other than turbulence has been responsible for the observed abundance distribution. Crawford et al. (2005) observed spatially coincident Hα and soft X-ray filaments surrounding the BCG and conclude that the structure of the filaments is inconsistent with turbulence at scales above a few kpc. Similar filaments are observed in the core of the Perseus cluster (Conselice et al. 2001) and spectroscopic measurements of their line-of-sight velocity (Hatch et. al. 2005, submitted) indicates that the velocity gradients of the filaments are smooth, which is a strong indication that the surrounding medium is not turbulent. Velocity measurements of a horseshoe-shaped filament located below a rising bubble are consistent with laminar flow induced by the bubble rising in a viscous fluid, as proposed by Fabian et al. (2003b) based on the filament shape. These observations suggest filaments may be dragged out of the cluster centre by the rising bubbles, a process that has also been implicated in reproducing observed features in the Perseus abundance map (Sanders et al. 2005). Since these motions are largely radial, they should be more efficient at redistributing the metals than turbulent motion and we can estimate a diffusion coefficient $D \sim v_{\mathrm{bubble}} r_{\mathrm{bubble}}$. Using the radii and buoyancy velocities from Dunn & Fabian (2004) as an estimate of r_{bubble} and v_{bubble}, we find a diffusion coefficient of $D \sim 2\times10^{29}\,\mathrm{cm^2 s^{-1}}$, which will be reduced by the fact that bubble related flows operate in only a fraction of the cluster core at a time. Spectroscopic measurements of the filaments in Centaurus are needed to confirm the flow pattern is similar to that in the Perseus cluster.

A second possibility is suggested by Fig. 4. It is clear that the the largest discrepancy between the observed abundance distribution and the naive abundance-following-light model occurs in the highly enriched region inside about 20 kpc. The metal injection into

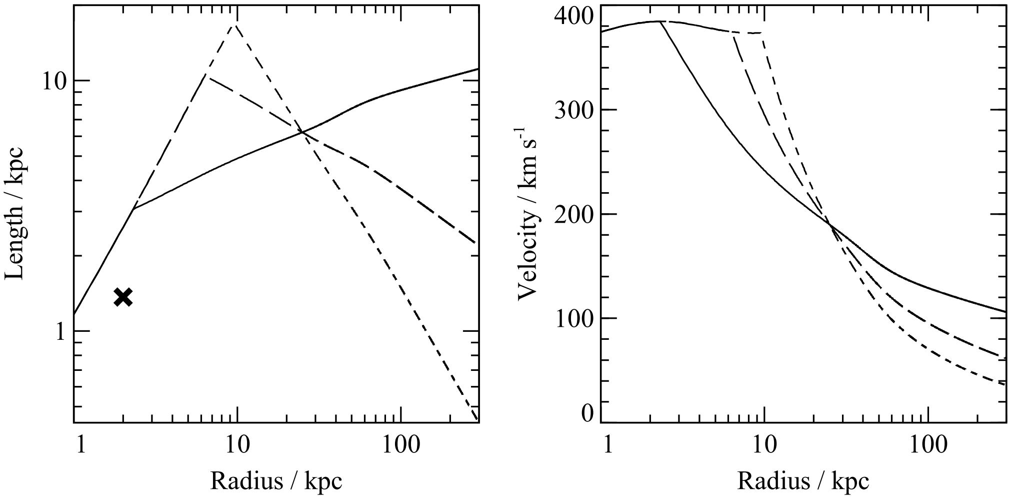

Figure 7. Length and velocity scales needed for turbulent diffusion to balance heating with in a model with $D_0 = 4\times10^{28}\,\mathrm{cm^2 s^{-1}}$, $r_0 = 25\,\mathrm{kpc}$ and $\alpha = 0$ (solid line), $\alpha = 1$ (dashed line) and $\alpha = 2$ (dot-dashed line). The cross indicates the position and average radius of the Centaurus bubbles (Dunn & Fabian 2004).

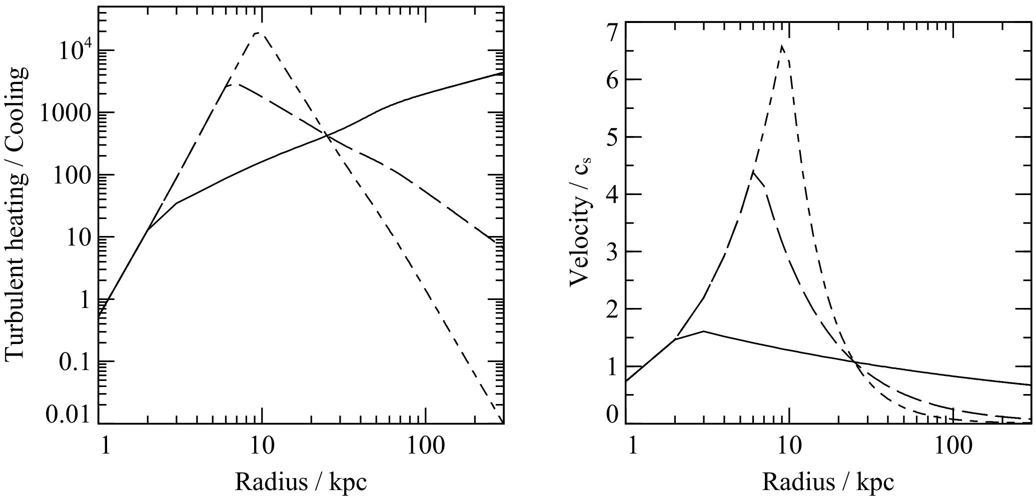

Figure 8. Heating rates as a fraction of the required heating and the velocity as a fraction of local sound speed, assuming $D = 0.11vl_{\max}$ (see text for definitions) in a model with $D_0 = 4\times10^{28}\,\mathrm{cm^2 s^{-1}}$, $r_0 = 25\,\mathrm{kpc}$ and $\alpha = 0$ (solid line), $\alpha = 1$ (dashed line) and $\alpha = 2$ (dot-dashed line).

these regions would enhance the cooling rate in these regions, potentially causing the gas to cool out of the X-ray band. The mass of this gas is of the order $10^8 M_\odot$, therefore this would not represent a substantial cooling rate over the lifetime of the cluster.

These results suggest the diffusion model may be systematically overestimating the level of turbulence. It should, however, be emphasised that the models of turbulent heating and diffusion are very coarse and so these results should be regarded as very approximate. In particular, the result that turbulent motion on the scale size of the bubble requires velocities close to or above the sound speed to reproduce the observed iron peak should be regarded as demonstrating the limitations of the purely stochastic model of metal spreading.

5.2 Turbulent Conduction

If we imagine the cluster as being divided into thin shells with each of the gas properties being constant within the shell, the conductivity required for heating to balance cooling is given by Voigt & Fabian (2004):

$$\kappa_j = \frac{\sum_{i=1}^{j} \Lambda(T_i, Z_i) n_i^2 \Delta V_i}{4\pi r_j^2 \left(\frac{dT}{dr}\right)_j}. \quad (9)$$

In the case of an unmagnetised plasma, the theoretical electron conductivity is given by the Spitzer form:

$$\kappa_{\mathrm{Spitzer}} = 640 \left(\frac{2\pi}{m_e}\right)^{\frac{1}{2}} \frac{k\varepsilon_0^2}{e^4} \frac{(kT)^{\frac{5}{2}}}{Z \ln\Lambda}, \quad (10)$$

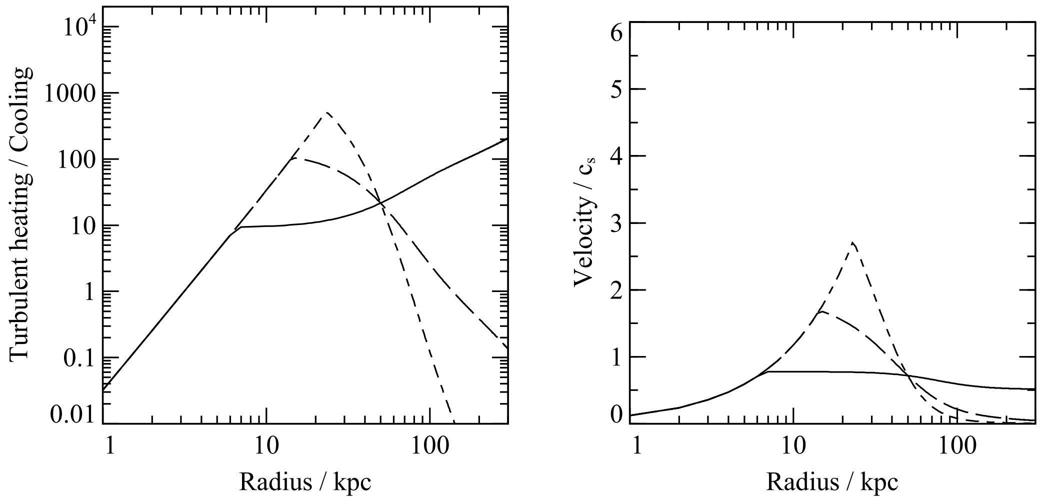

Figure 9. As Fig. 8 but for the Perseus cluster using the results of Rebusco et al. (2005); $D_0 = 2\times10^{29}\,\mathrm{cm^2s^{-1}}$, $r_0 = 50\,\mathrm{kpc}$ and $\alpha = 0$ (solid line), $\alpha = 1$ (dashed line) and $\alpha = 2$ (dot-dashed line).

where Λ (not to be confused with the cooling function) is the coulomb logarithm:

$$\ln\Lambda \approxeq 37.8 + \ln\left[\left(\frac{T}{10^8 K}\right)\left(\frac{n_e}{10^{-3}\mathrm{cm}^{-3}}\right)\right]. \qquad (11)$$

In practise the conductivity is likely to be suppressed by the presence of magnetic fields which bind electrons to field lines and so greatly reduce the effectiveness of transport perpendicular to the local field direction. The overall degree of suppression is therefore strongly dependent on the field geometry in the cluster centre. In the case of a turbulent magnetic field, Narayan & Medvedev (2001) find that the effective conductivity is about one fifth the Spitzer value.

In the case of a turbulent gas, the thermal conductivity κ is given by $\kappa_{\mathrm{turb}} = n_e k D$ Cho et al. (2003). Fig. 10 shows the thermal conductivity required to balance conduction in Centaurus with the Spitzer conductivity and the turbulent conductivity derived from the diffusion model in Fig. 6. The turbulent conductivity is lower than the required conductivity everywhere in the cluster. However, it appears that Spitzer electron conductivity may be significant in the outer regions of the cluster, although this depends on the degree of suppression due to the magnetic field.

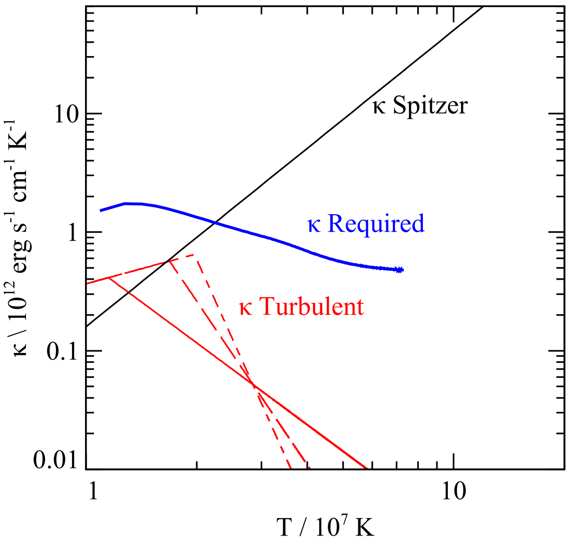

Figure 10. Level of turbulent conduction compared to the required conduction for the cluster (solid blue line) and the Spitzer electron conductivity (solid black line). Turbulent diffusion is based on the diffusion model with $D_0 = 4\times10^{28}\,\mathrm{cm^2s^{-1}}$, $r_0 = 25\,\mathrm{kpc}$ and $\alpha = 0$ (solid red line), $\alpha = 1$ (dashed line) and $\alpha = 2$ (dot-dashed line). In all cases, the level of conductivity due to turbulent diffusion is below the conductivity required to balance heating.

6 CONCLUSIONS

The observed central abundance peak in the Centaurus cluster can be approximately reproduced by diffusive spreading of metals ejected from the BCG. The boxy abundance profile favours a model where the diffusion coefficient declines away from the centre; this is qualitatively consistent with the gas motions resulting from the rising radio bubbles observed in the cluster core. In particular, reproducing the sharp observed abundance drop requires a diffusion coefficient of $D < 4\times10^{28}\,\mathrm{cm^2s^{-1}}$ for $r > 25\,\mathrm{kpc}$ and hence the velocity field must be relatively quiet in this region. This is a robust result and our main conclusion.

We have calculated approximate length and velocity scales for turbulent motion to heat the cluster. They predict length scales of up to $\sim 10\,\mathrm{kpc}$ and velocities of up to $\sim 400\,\mathrm{km s^{-1}}$ in the inner $\sim 25\,\mathrm{kpc}$. That this length scale is larger than the bubble scale is a remaining difficulty as a substantial reduction in the length scale of the motion implies a reduction of the diffusion coefficient, producing a poorer fit to the data, or a large increase in the turbulent velocity. This suggests that the level of turbulence may not be as high as predicted. Spreading of metals in the region $r < 25\,\mathrm{kpc}$ may be due to some other process such as the velocity flow behind rising bubbles. More work is needed to quantify how effective such a mechanism can be. With the next generation of X-ray spectrometers, direct measurements of turbulent velocities will be possible and will place strong constraints on the model.

The thermal conductivity arising from turbulent mixing has also been calculated and this has been shown to be insignificant except, perhaps, in the very central regions of the cluster.

ACKNOWLEDGEMENTS

JG acknowledges support from PPARC and RGM thanks PPARC for support whilst at Cambridge. ACF thanks the Royal Society for support. Work supported in part by the U.S. Department of Energy under contract number DE-AC02-76SF00515.

REFERENCES

Allen S. W., Fabian A. C., 1994, MNRAS, 269, 409
Allen S. W., Schmidt R. W., Fabian A. C., 2001, MNRAS, 328, L37
Anders E., Grevesse N., 1989, Geochim. Cosmochim. Acta, 53, 197
Arnaud K. A., 1996, in ASP Conf. Ser. 101: Astronomical Data Analysis Software and Systems V, p. 17
Bîrzan L., Rafferty D. A., McNamara B. R., Wise M. W., Nulsen P. E. J., 2004, ApJ, 607, 800
Böhringer H., Matsushita K., Churazov E., Finoguenov A., Ikebe Y., 2004, A&A, 416, L21
Böhringer H., Voges W., Fabian A. C., Edge A. C., Neumann D. M., 1993, MNRAS, 264, L25
Cho J., Lazarian A., Honein A., Knaepen B., Kassinos S., Moin P., 2003, ApJ, 589, L77
Churazov E., Forman W., Jones C., Sunyaev R., Böhringer H., 2004, MNRAS, 347, 29
Churazov E., Gilfanov M., Forman W., Jones C., 1999, ApJ, 520, 105
Churazov E., Sunyaev R., Forman W., Böhringer H., 2002, MNRAS, 332, 729
Conselice C. J., Gallagher J. S., Wyse R. F. G., 2001, AJ, 122, 2281
Crawford C. S., Hatch N. A., Fabian A. C., Sanders J. S., 2005, MNRAS, 363, 216
De Grandi S., Ettori S., Longhetti M., Molendi S., 2004, A&A, 419, 7
Dennis T. J., Chandran B. D. G., 2005, ApJ, 622, 205
Dunn R. J. H., Fabian A. C., 2004, MNRAS, 355, 862
Edge A. C., Stewart G. C., 1991, MNRAS, 252, 414
Fabian A. C., 1994, ARA&A, 32, 277
Fabian A. C., Celotti A., Blundell K. M., Kassim N. E., Perley R. A., 2002, MNRAS, 331, 369
Fabian A. C., Sanders J. S., Allen S. W., Crawford C. S., Iwasawa K., Johnstone R. M., Schmidt R. W., Taylor G. B., 2003a, MNRAS, 344, L43
Fabian A. C., Sanders J. S., Crawford C. S., Conselice C. J., Gallagher J. S., Wyse R. F. G., 2003b, MNRAS, 344, L48
Fabian A. C., Sanders J. S., Taylor G. B., Allen S. W., 2005, MNRAS, 360, L20
Finoguenov A., David L. P., Ponman T. J., 2000, ApJ, 544, 188
Fukazawa Y., Kawano N., Kawashima K., 2004, ApJ, 606, L109
Hashimoto Y., Barcons X., Böhringer H., Fabian A. C., Hasinger G., Mainieri V., Brunner H., 2004, A&A, 417, 819
Hernquist L., 1990, ApJ, 356, 359
Lauberts A., Valentijn E. A., 1989, The surface photometry catalogue of the ESO-Uppsala galaxies. Garching: European Southern Observatory, —c1989
Liedahl D. A., Osterheld A. L., Goldstein W. H., 1995, ApJ, 438, L115
Mathews W. G., Brighenti F., Buote D. A., Lewis A. D., 2003, ApJ, 596, 159
McNamara B. R. et al., 2000, ApJ, 534, L135
Mewe R., Gronenschild E. H. B. M., van den Oord G. H. J., 1985, A&AS, 62, 197
Mushotzky R. F., Loewenstein M., 1997, ApJ, 481, L63
Narayan R., Medvedev M. V., 2001, ApJ, 562, L129
Paturel G., Petit C., Prugniel P., Theureau G., Rousseau J., Brouty M., Dubois P., Cambresy L., 2003, VizieR Online Data Catalog, 7237
Peterson J. R., Fabian A. C., 2005, arXiv:astro-ph/0505517
Peterson J. R., Kahn S. M., Paerels F. B. S., Kaastra J. S., Tamura T., Bleeker J. A. M., Ferrigno C., Jernigan J. G., 2003, ApJ, 590, 207
Pringle J. E., 1989, MNRAS, 239, 479
Read A. M., Ponman T. J., 2003, A&A, 409, 395
Rebusco P., Churazov E., Böhringer H., Forman W., 2005, MNRAS, 359, 1041
Renzini A., Ciotti L., D'Ercole A., Pellegrini S., 1993, ApJ, 419, 52
Ruszkowski M., Brüggen M., Begelman M. C., 2004, ApJ, 615, 675
Sanders J. S., Fabian A. C., 2002, MNRAS, 331, 273
Sanders J. S., Fabian A. C., Allen S. W., Schmidt R. W., 2004, MNRAS, 349, 952
Sanders J. S., Fabian A. C., Dunn R. J. H., 2005, MNRAS, 360, 133
Schuecker P., Finoguenov A., Miniati F., Böhringer H., Briel U. G., 2004, A&A, 426, 387
Spitzer L., 1956, Physics of Fully Ionized Gases. Physics of Fully Ionized Gases, New York: Interscience Publishers, 1956
Tabor G., Binney J., 1993, MNRAS, 263, 323
Tozzi P., Rosati P., Ettori S., Borgani S., Mainieri V., Norman C., 2003, ApJ, 593, 705
Vogt C., Enßlin T. A., 2005, A&A, 434, 67
Voigt L. M., Fabian A. C., 2004, MNRAS, 347, 1130
White D. A., 2000, MNRAS, 312, 663